# SUPERCONDUCTIVITY - Applied

## Application of a Nb Hot-Electron Bolometer for Time-Resolved Electron Magnetic Resonance

Araujo, H.M., QMC Instruments Ltd. and Queen Mary and Westfield College, UK, Physics
van Tol, J., NHMFL
Wood, K., QMC Instruments Ltd., UK

For high frequency, time-resolved electron magnetic resonance (EMR), the detector is a critical factor and should combine fast response and high sensitivity over a broad frequency range. The current detector at the NHMFL for time-resolved EMR is a heterodyne Schottky-diode mixer, which gives both fast response (< ns) and high sensitivity, but this type of detector has to be optimized for a single frequency, and its performance goes down at higher frequencies. From this perspective, the use of a direct detector covering all the frequencies that are likely to be used in high frequency EMR would have great advantages. We have therefore tested a phonon-cooled Nb hot-electron bolometer (HEB), which is sensitive from the far-infrared to the millimeter-wave region, in the actual EMR spectrometer.

Two things were to be determined: sensitivity and the response time. The optical Noise-Equivalent-Power (NEP) at 240 GHz of the detector was found to be $10^{-11}$ W/√Hz, and in an actual CW-EMR experiment at 240 GHz, the signal-to-noise ratio was about a factor 20 smaller than the same signal measured with a Schottky diode mixer. It should be noted that the Nb-HEB geometry was not optimized for this frequency, but still an improvement in sensitivity of at least two orders of magnitude would be necessary to make this device compete with the Schottky detectors.

We observed the response of the Nb-HEB detector to a change in incident intensity induced by an optical switch, consisting of a Si-wafer in the millimeter-wave beam path that can be illuminated by a Nd-Yag pulsed-laser. The effect of a laser pulse on the Si is a very fast decrease in transmission (<600 ps), followed by a much slower increase of the order of (20 μs). The time-resolved signal, observed with the Nb-HEB bolometer indeed shows the expected fast response of the order of 1 ns corresponding to the hot-electron bolometric effect. However, also a slower (~1 μs) component of the same order of magnitude is present in the Nd-HEB response. The origin of this response is likely related to the ordinary bolometric response of the element, possibly substrate-induced. We conclude that the Nb HEB detector could play a role in future high field, time-resolved EMR applications, but that improvements in sensitivity and flatness of the frequency response have to be made.

## $BaZrO_3$ Insulation Coatings by Sol-Gel Technique for HTS Coils

Celik, E., NHMFL and Sakarya Univ., Turkey, Metallurgy
Mutlu, I.H., NHMFL and Harran Univ., Turkey, Physics
Akin, Y., NHMFL/UF, Material Science and Engineering
Okuyucu, H., NHMFL and Gazi Univ., Turkey, Metallurgy
Sigmund, W., UF, Material Science and Engineering
Hascicek, Y.S., NHMFL

The $ZrO_2$ based insulation coatings were successfully applied on Ag or AgMg/Bi-2212 superconducting tapes using sol-gel technique for a 3.0 T HTS insert coil at the NHMFL. A Bi-2212 wind-and-react insert magnet consisting of three concentric sections was built and generated 3.0 T in a 19.0 T back-ground magnetic field.[1] The NHMFL's reel-to-reel sol-gel insulation coating process provides thin and robust enough high temperature insulation for W&R superconducting magnets. In addition to this, this insulation system has been used for BiPb2232 coils built from already reacted conductors to increase the packing

density. Also, effectiveness of insulation materials is a very important parameter in minimizing the leaks and resistance to reactions during the melt-process. Due to these facts, $ZrO_2$, MgO-$ZrO_2$, $Y_2O_3$-$ZrO_2$, $CeO_2$-$ZrO_2$, $Sm_2O_3$-$ZrO_2$, $Er_2O_3$-$ZrO_2$, $In_2O_3$-$ZrO_2$, and $SnO_2$-$ZrO_2$ coatings were developed and used to insulate Ag or AgMg sheathed Bi-2212 tapes.[2] In this work, processing, structure, and electrical properties of $BaZrO_3$ (BZO) insulation coatings on Ag or AgMg sheathed Bi-2212 tapes were studied.

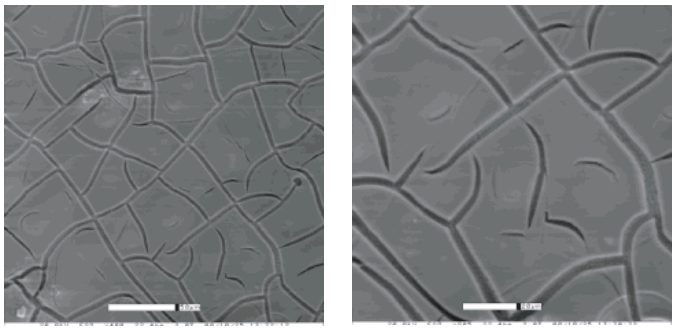

**Figure 1.** SEM micrographs of BZO coatings on AgMg sheathed Bi-2212 tapes heat treated at 600° C for 30 min in air.

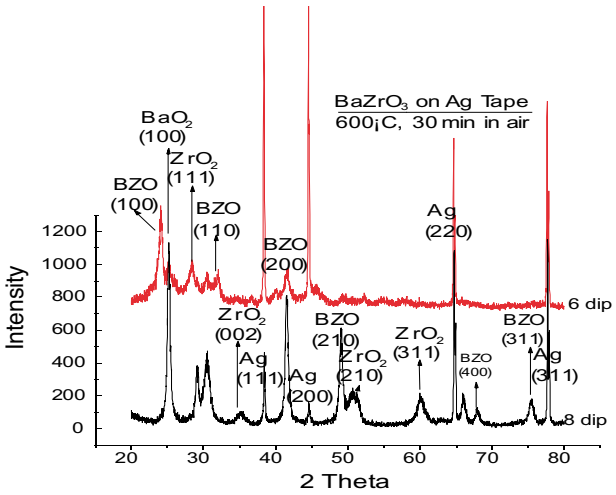


**Figure 2.** XRD patterns of BZO coatings on Ag tapes heat treated at 600° C for 30 min in air at 6 and 8 dips.

BZO coatings were produced on Ag and Ag sheathed Bi-2212 tapes supplied by Oxford Superconducting Technology, Inc., using a continuous, reel-to-reel sol-gel technique for HTS high field insert magnet. The chelation and complexation ratios of solutions were 3.1 and 0.58, respectively. The coating process consists of dipping, drying, burnt-out, oxidation, and bonding of coating to substrate. The amorphous structure was oxidized in the temperature range of 450° C and 550° C. The total thickness of the resulting coatings was approximately 4 μm after annealing process. SEM observations showed a maze of cracks in the BZO insulation coatings. Cubic BZO, cubic $BaO_2$, and cubic $ZrO_2$ phases were observed in the XRD of BZO coatings. The average resistance of the BZO coatings was 11 Mohms after 2 dipping. The dielectric constant and the high voltage breakdown values of the BZO coatings on Ag tape after 10 dipping is approximately 22.5 and 0.98 kV at 1.5 mA, respectively.

[1] Weijers, H.W., *et al.*, IEEE Trans. on App. Sup., **9**, 563-566 (1999).
[2] Celik, E., *et al.*, Physica C, **340**, 193-202 (2000).

## Effect of Composition on the Upper Critical Field for $Nb_3Sn$ Conductors Made by the Modified Jelly Roll Process

Parrell, J., Oxford Instruments, Inc.,
Superconducting Technology (OI-ST)
Hentges, R., OI-ST
Zhang, Y., OI-ST
Hong, S., OI-ST
Field, M., OI-ST

Oxford Instruments, Inc., Superconducting Technology has been manufacturing $Nb_3Sn$ conductors for many years using both bronze processes as well as internal tin. One manufacturing route used at OI-ST for internal tin wires is the modified jelly roll process (MJR). For this process, we start by wrapping expanded niobium, or niobium alloy around a tin, or tin alloy rod. This assembly is inserted into a copper can and processed into hexagon shaped rods. The hexes are further re-stacked into a copper can and drawn to the final wire. This process allows for rapid study of alloy combinations by changing the alloying elements and concentrations of the individual components.

The upper critical field ($B_{c2}$) of $Nb_3Sn$ can be improved by the proper element additions to $Nb_3Sn$.[1]

For this reason, $Nb_3Sn$ composites are often fabricated with niobium alloyed with small amounts of additives such as titanium or tantalum. Tin alloyed with titanium is commonly used in internal tin processes. We have tried to find an optimum combination of material for high upper critical field by taking advantage of the easy prototyping capability of the MJR process.

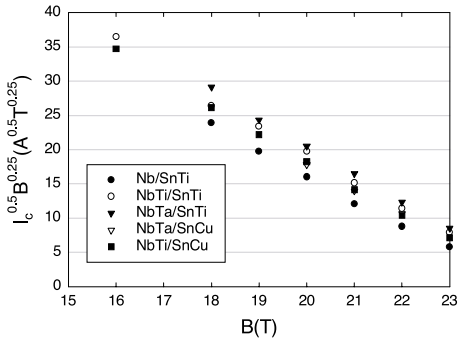


**Figure. 1.** Kramer plot of $Nb_3Sn$ with additive variation. The combination of Nb-Ta and Sn-Ti performs best at high field.

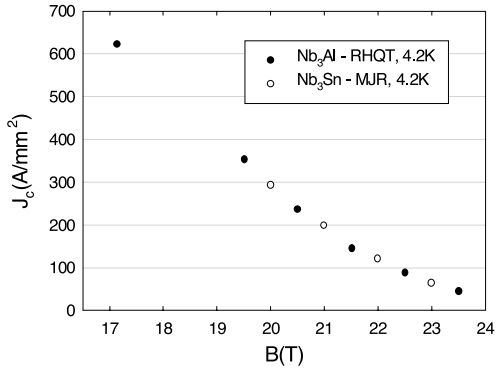


**Figure. 2**. MJR-$Nb_3Sn$ critical current density (Non-Cu) compared to $Nb_3Al$ fabricated rapid heating, quenching, and transformation. The two materials have nearly identical performance.

We made five composites with different combinations of filament and tin core alloys: (1) Nb with Sn-2wt%Ti, (2) Nb-0.8wt%Ti with Sn-0.7wt%Cu, (3) Nb-7.5wt%Ta with Sn-0.7%Cu, (4) Nb-0.8wt%Ti with Sn-2wt%Ti, and (5) Nb-7.5wt%Ta and Sn-2wt%Ti. These composites were reduced to the same final diameter and were given the same heat treatment. The samples' critical currents were measured at the NHMFL up to 23 T. We compare their Kramer numbers[2] in Fig. 1, and while these values are fairly close, there is an indication that the Nb-Ta/Sn-Ti combination yields a higher $B_{c2}$. This enhancement in $B_{c2}$ is of great benefit for magnets to be operated at very high fields, and extends the capable field range of $Nb_3Sn$. We note the recent developments of very attractive critical current densities at high field in $Nb_3Al$ strand made by the rapid heating, quenching, and transformation (RHQT) method,[3] and show in Fig. 2 that the non-Cu $J_c$ of recent MJR strand is comparable to RHQT $Nb_3Al$ strand.

[1] Suenaga, M., *et al.,* Appl. Phys. Lett., **44**, 919 (1984).
[2] Kramer, E.J., J. Appl. Phys., **44**, 1360-1370 (1973).
[3] Takeuchi, T., "$Nb_3Al$-Rapid Heating, Quenching and Transformation Process," presented at MT-16 (1999).

## Electrical Characterization of Ceramic Insulation Coatings for Magnet Technology

Mutlu, I.H., NHMFL and Harran Univ., Turkey, Physics
Celik, E., NHMFL and Sakarya Univ., Turkey, Metallurgy
Okuyucu, H., NHMFL and Gazi Univ., Turkey, Metallurgy
Hascicek, Y.S., NHMFL

$ZrO_2$ based coatings have been insulated on Ag and AgMg/Bi-2212 superconducting tapes and wires using sol-gel technique for high field insert magnets at the NHMFL. Insulating materials surrounding the conductors are used to prevent electric short circuits within the winding of a coil. $ZrO_2$ and stabilized $ZrO_2$ coatings are available for high temperature insulation because of chemical stability, high resistivity, and a large relative dielectric constant. The large dielectric constant of $ZrO_2$ ($\varepsilon \cong 20$) provides good insulation without short circuits.[1] In this work, high temperature insulation coatings were prepared on Ag and AgMg/Bi-2212 tapes by a sol-gel method. The electrical properties of the coatings were studied.

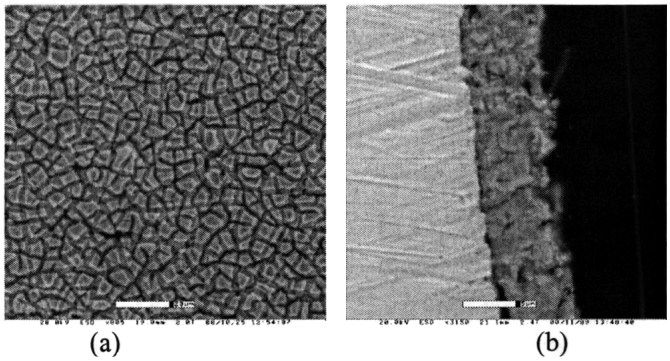


**Figure 1.** SEM micrographs of (a) surface and (b) cross-section of $Y_2O_3$-$ZrO_2$ on AgMg sheathed Bi-2212 tapes.

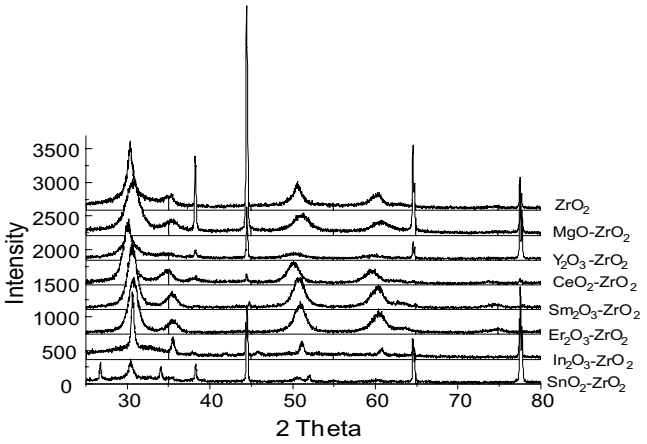


**Figure 2.** XRD patterns of $ZrO_2$, MgO-$ZrO_2$, $Y_2O_3$-$ZrO_2$, $CeO_2$-$ZrO_2$, $Sm_2O_3$-$ZrO_2$, $Er_2O_3$-$ZrO_2$, $In_2O_3$-$ZrO_2$, and $SnO_2$-$ZrO_2$ coatings on Ag tapes as marked.

$ZrO_2$, MgO-$ZrO_2$, $Y_2O_3$-$ZrO_2$, $CeO_2$-$ZrO_2$, $Sm_2O_3$-$ZrO_2$, $Er_2O_3$-$ZrO_2$, $In_2O_3$-$ZrO_2$, and $SnO_2$-$ZrO_2$ insulation coatings were produced on Ag and AgMg sheathed Bi-2212 superconducting tapes, and Cu-$Nb_3Sn$ wires by reel-to-reel sol-gel process using $Zr[O(CH_2)_3CH_3]_4$ as main precursor (Fig. 1). Cubic, orthorombic, and tetragonal phases were observed on the XRD patterns for $ZrO_2$ and $ZrO_2$ based coatings (Fig. 2). Dielectric constant and high voltage breakdown values of $ZrO_2$, MgO-$ZrO_2$, $Y_2O_3$-$ZrO_2$, $CeO_2$-$ZrO_2$, $Sm_2O_3$-$ZrO_2$, $Er_2O_3$-$ZrO_2$, $In_2O_3$-$ZrO_2$, and $SnO_2$-$ZrO_2$ coatings increased as the number of dipping increased (Fig. 3). The high voltage breakdown values for $ZrO_2$, MgO-$ZrO_2$, $Y_2O_3$-$ZrO_2$, $CeO_2$-$ZrO_2$, $Sm_2O_3$-$ZrO_2$, and $Er_2O_3$-$ZrO_2$ coatings were about 1 kV at 10 mA. The maximum dielectric constant, 26, was obtained in MgO-$ZrO_2$.

[1] Celik, E., *et al.*, Patent Application, May (1998).

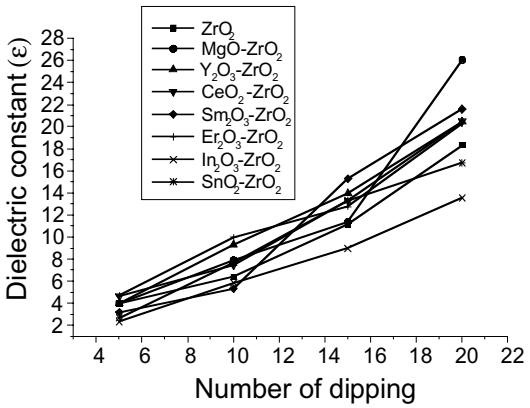


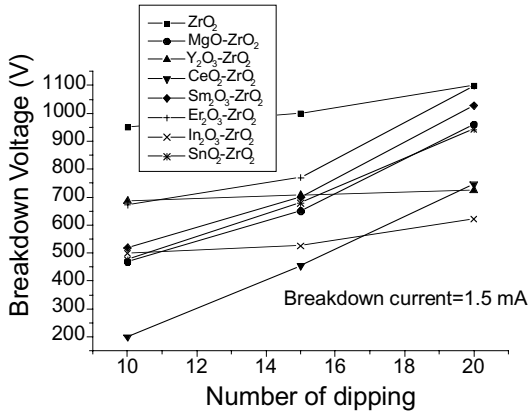


**Figure 3.** (a) Dielectric constant and (b) high voltage breakdown versus number of dippings for insulation coatings which was annealed at 850 °C for 20 hours under $O_2$ flow.

## Non-Vacuum YBCO Coated Conductor Development

Mutlu, I.H., NHMFL and Harran Univ., Turkey, Physics
Celik, E., NHMFL and Sakarya Univ., Turkey, Metallurgy
Okuyucu, H., NHMFL and Gazi Univ., Turkey, Metallurgy
Ramazanoglu, M.K., FSU, Physics
Akin, Y., UF, Materials Science and Engineering
Sigmund, W., UF, Materials Science and Engineering
Crow, J.E., NHMFL
Hascicek, Y.S., NHMFL

Sol-gel deposition of $YBa_2Cu_3O_{7+x}$ (YBCO) holds great potential as a fast and efficient method of producing large-scale, biaxially-textured films at a lower cost than physical and chemical vapor

deposition techniques. At the NHMFL, we have been using sol-gel for about seven years for high temperature insulation coatings and for YBCO coated conductor development for the last two years.[1] However, one difficulty in applying sol-gel processing such as metal-organics (alkoxides, acacetates, etc.) dissolved in alcohols, organic acids, and ethers, is the need for an organic pyrolysis step prior to YBCO formation to remove the bound carbonaceous species.

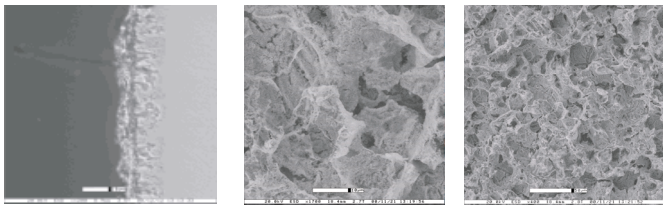

**Figure 1.** SEM micrographs of (a) cross-section of the film, (b) and (c) $Gd_2O_3$ buffer layer and YBCO on Ni tape.

In this study, YBCO films were prepared on textured $Gd_2O_3$, $Er_2O_3$ and NiO buffer layered Ni tapes by a continuous, reel-to-reel sol-gel technique using solutions that were prepared from various precursors of Y, Ba, and Cu. Microstructure and $T_c$ dependence on stoichiometry in YBCO films and solutions were investigated.[1] Thick, crack-free, pinhole-free sol-gel YBCO layers were grown on textured $Gd_2O_3$, $Er_2O_3$ and NiO buffer layered Ni substrate tapes, in order to characterize the stoichiometry, structure, and morphology (Fig. 1). YBCO crystallites appear quite dense at the surface of a sample that was heat treated at 850° C for 0.5 h under $O_2$-Ar flow. A sol-gel YBCO surface coated conductor on to the buffer layered Ni tape has been realized using a reel-to-reel, continuous set-up with a three zones furnace. SEM, XRD (Fig.2), and resistance measurements show that almost phase pure, thick (~6 μm) YBCO layers can be realized on buffered rolled Ni tape. Fig. 3 shows R-T curve for a sol-gel YBCO coated conductor. The onset of the critical temperature ($T_c$) was measured to be 92 K.

$J_c$ of this coated conductor was $10^5$ A/cm$^2$ at 4.2 K and self field. We are working on improving $J_c$ by way of improving texture and surface quality of buffer layers, and texture and phase purity in YBCO layers.

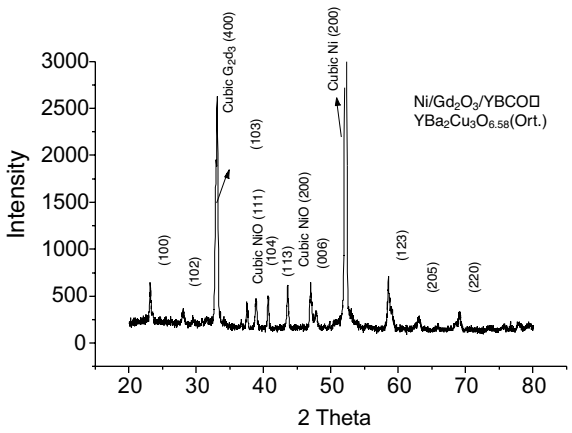


**Figure 2.** The XRD pattern of YBCO on $Gd_2O_3$, buffered Ni tapes.

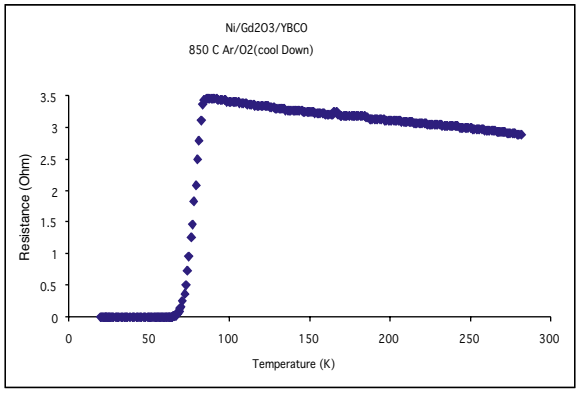


**Figure 3.** A typical R-T curve for a sol-gel YBCO coated conductor.

[1] Mutlu, I.H., *et al.,* IEEE Trans. App.Sup., **10**, 1154-1157 (2000).

## Preparation of $Gd_2O_3$ and $Er_2O_3$ Buffer Layers for YBCO Conductors by Continuous Sol-Gel Process

Okuyucu, H., NHMFL and Gazi Univ., Turkey, Metallurgy
Celik, E., NHMFL and Sakarya Univ., Turkey, Metallurgy
Ramazanoglu, M.K., NHMFL/FSU, Physics
Akin, Y., NHMFL/UF, Materials Science & Metallurgy
Mutlu, I.H., NHMFL and Harran Univ., Turkey, Physics
Sigmund, W., UF, Materials Science Engineering
Crow, J.E., NHMFL
Hascicek, Y. S., NHMFL

$Gd_2O_3$ and $Er_2O_3$ films were deposited on cube-textured Ni substrates by reel-to-reel non-vacuum sol-gel technique for $YBa_2Cu_3O_{7-x}$ (YBCO) coated conductors. Their microstructures were observed by environmental scanning electron microscopy (ESEM), and their crystallographic texture and surface roughness evaluated by X-ray diffraction (XRD), pole figure, and atomic force microscopy (AFM).

$Gd_2O_3$ and $Er_2O_3$ were heat treated for texture development at 1150° C for 10 minutes under 2% $H_2$-Ar flow. The θ/2θ scan for single coat $Gd_2O_3$ and $Er_2O_3$ shown in Fig. 1. The peak at 2θ of 33.113° belongs to the cubic $Gd_2O_3$ phase, the peak at 2θ of 33.967° belongs to the cubic $Er_2O_3$ phase, and both peaks are indexed to be the (400) reflection.

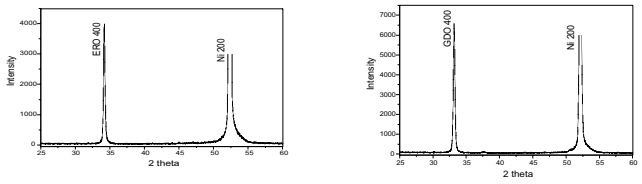


**Figure 1.** XRD patterns of single coat $Er_2O_3$ and $Gd_2O_3$ layers.

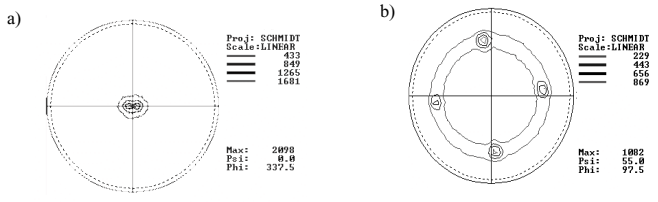


**Figure 2.** The pole figures of $Er_2O_3$ and $Gd_2O_3$; a) $Er_2O_3$ (400) b) $Gd_2O_3$ (222).[1]

The texture measurements were carried out on $Er_2O_3$ and $Gd_2O_3$ films heat-treated at 1150° C for 10 min. under 2%$H_2$-Ar flow. The pole figure (Fig. 2) of the $Er_2O_3$ and $Gd_2O_3$ sol_gel buffer layer showed a single cube-on-cube epitaxy on the textured Ni (100) substrate. From the pole figure, we can conclude that the $Er_2O_3$ and $Gd_2O_3$ films exhibit a biaxial alignment on the Ni (100) substrate. We are currently working on increasing the batch length, as well as developing continuous coating and texturing set up.

[1] Okuyucu, H., *et al.,* "Textured Buffer Layers for YBCO Coated Conductors by Continuous Sol-Gel Processing," ASC Conference, Virginia Beach, VA, September 17-22, 2000.

## Systematic Study of Grain Boundary Grooving on Textured Ni Substrates for Coated Conductors

Okuyucu, H., NHMFL and Gazi Univ., Turkey, Metallurgy
Ramazanoglu, M.K., NHMFL/FSU, Physics
Crow, J.E., NHMFL
Hascicek, Y.S., NHMFL

The effects of annealing of Ni substrates for YBCO coated conductors on grain size, grain boundary grooving, and surface smoothness were studied systematically. Ni substrates were annealed at temperatures between 800° C and 1050° C, under 4% $H_2$-Ar flow for varying times totaling 18 different heat treatments. During annealing of Ni, in addition to developing the desired cube texture, the surfaces of the individual grains may roughen, and the grain boundaries become grooved, see Fig. 1. As seen in Fig. 2, Nickel grain size doesn't show much variation for the heat treatment conditions studied.

Depth of grain boundary grooving seems to fall between 80 nm and 250 nm for the heat treatment

conditioned studied. These may be too rough to grow epitaxial buffer layers on. We plan to find the optimum conditions for acceptable grain boundary grooving and texture.

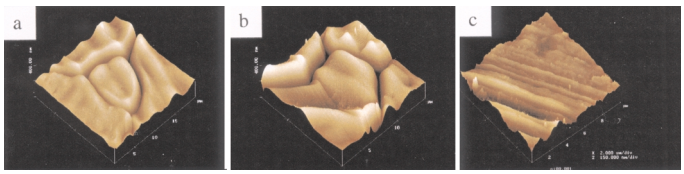


**Figure 1.** AFM surface topography of Ni substrate: (a) annealed at 950° C for 60 min, (b) annealed at 1050° C for 20 min, and (c) as rolled. All the images are 20 µm x 20 µm and the vertical scale is 400 nm.

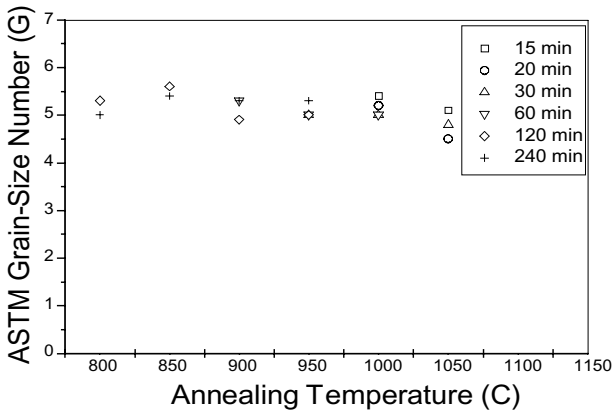


**Figure 2.** Grain size distribution of Ni for different annealing times and temperatures.

## High Performance $Nb_3Sn$(Ta) by Tin Enrichment and Increased Filament Content

Pourrahimi, S., Superconducting Systems, Inc., R&D

This was a Phase I SBIR program funded by the office of High Energy Physics of the Department of Energy. Powder metallurgy was used to establish an innovative, practical, and economical method of fabricating high performance $Nb_3Sn$ wires. Bitter magnets at the NHFML were used to characterize the critical current density ($J_c$) of various prototype wires in background magnetic fields of up to 18 T. Preliminary results indicated that "non-copper" $J_c$ of more than 2000 A/mm$^2$ in background fields of 15 T may be achieved. Fig. 1 shows the cross section of a typical wire processed for this program. Sample wires were tin plated to increase the tin content of the wires. Phase II of the program is currently underway.

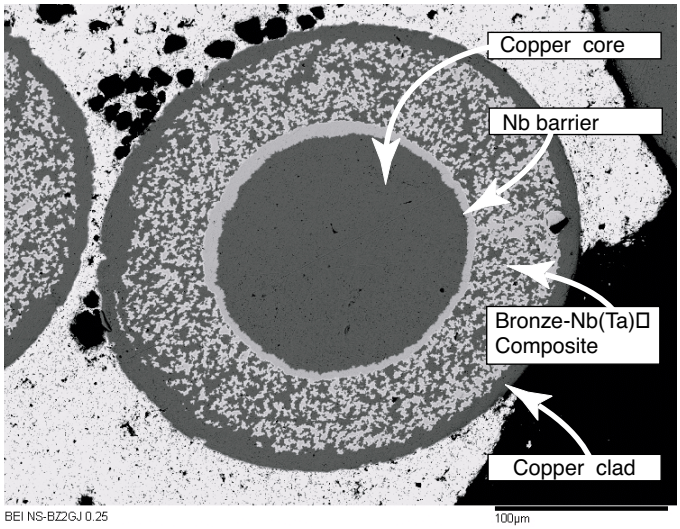


**Figure 1.** A bronze matrix multifilamentary $Nb_3Sn$ wire produced by powder metallurgy.

## Optimization of Heat Treatment Conditions for AgMg-Clad Bi2212 Superconducting Tapes Used for 5 T Insert Magnets

Sastry, P.V.P.S.S., NHMFL
Celik, E., NHMFL
Mutlu, I., NHMFL
Akin, Y., NHMFL
Trociewitz, U.P., NHMFL
Weijers, H.W., NHMFL
Hascicek, Y.S., NHMFL
Schwartz, J., NHMFL
Miao, H., Oxford Superconducting Technology, U.S.A.
Marken, K., Oxford Superconducting Technology, U.S.A.
Hong, S., Oxford Superconducting Technology, U.S.A.

After the successful demonstration of a Bi2212 insert magnet that generated a field of 3 T in a background field of 19 T in 1999, we started

addressing the issues for extending the technology to build a 5 T Bi2212 magnet using HTS conductor supplied by Oxford Superconducting Technology. In the 5 T magnet, all of the conductor will be based upon powder-in-tube, AgMg-clad, Bi-2212 technology. In the 3 T magnet, the conductor had typical dimensions of 3.0 mm x 0.2 mm. To increase $I_c$ to values > 500 A, the conductor for the 5 T magnet is wider with typical dimensions of 5.0 mm x 0.2 mm and 6.0 mm x 0.2 mm. The superconductor to silver ratio in the new conductor is also higher than the conductor used for the 3 T magnet.

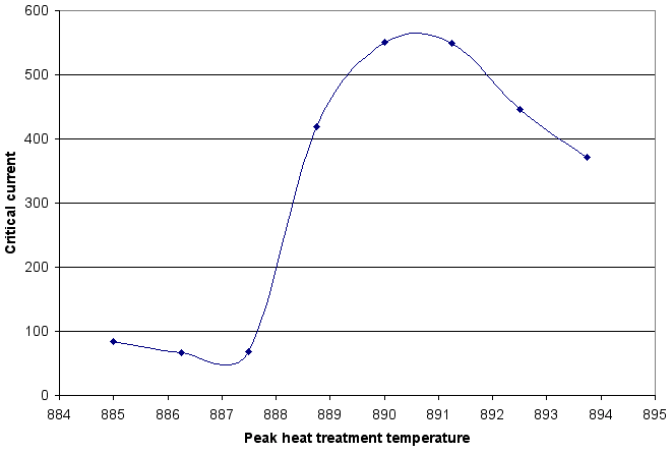


**Figure 1.** Peak heat treatment temperature versus critical current density of a AgMg-clad Bi2212 conductor.

Here, we report on heat treatment optimization of AgMg-Bi2212 conductor, focusing on the new issues that arise from increased conductor width, length per coil, and coil size. The partial melt processing protocol has been optimized for several batches of AgMg-Bi2212 conductor with varying widths. Fig. 1 depicts a typical plot of partial melt processing temperature versus $I_c$ for a 5 mm wide conductor. These studies are aimed at understanding the need for variation in required heat treatment conditions for achieving the optimum transport properties in conductors with varying dimensions.

## Synthesis and Characterization of $(Hg_{0.8}Re_{0.2})Ba_2CaCu_2O_{6+\delta}$ Thick Films on Ag Obtained by a Two-Step Dip-Coating/Rolling Method

IHRP

Su, J.H., NHMFL/FAMU-FSU College of Engineering
Sastry, P.V.P.S.S., NHMFL
Schwartz, J., NHMFL/FAMU-FSU College of Engineering

$(Hg_{0.8}Re_{0.2})Ba_2CaCu_2O_{6+\delta}$ ((Hg,Re)1212) thick films were fabricated by a two-step method of dip-coating and rolling $Re_{0.2}Ba_2Ca_2Cu_3O_{7+\delta}$ precursor onto Ag. To obtain optimal Hg and $O_2$ partial pressure, the precursor films were buried in the $Ba_2Ca_2Cu_3O_7$ precursor powders, and reacted in vacuum-sealed quartz tubes using $CaHgO_2$ as the external Hg source. The process details were given previously.[1] High phase purity (Hg,Re)1212 thick film, see Fig. 1, with colonies of aligned dense grains has been achieved, characterized by an onset transition temperature of 118 K.

The microstructure of (Hg,Re)1212 close to the silver interface is characterized by flat, textured superconducting grains (Fig. 2). One of the major reasons for texture development in the silver-superconductor interface during sintering is the very high surface diffusion coefficient of metallic silver in comparison with the superconductor. An investigation of the magnetization hysteresis loop widths at 10 K was conducted. We compared an as-prepared film and the film after the layer of superconducting material was removed from the free surface. It was shown that more than 60% signal comes from the layer close to the interface. Thus, one may conclude that the major contribution to $I_c$ comes from the thin layer close to the interface.

The microstructure of the polished transverse cross-section of a (Hg,Re)1212 thick film shows the film thickness is inhomogeneous along the silver surface, ranging from 2 μm to 20 μm and averaging ~ 15 μm. The critical transport current of this film was 1.6 A at 4.2 K, self field (Fig. 3). From the estimated

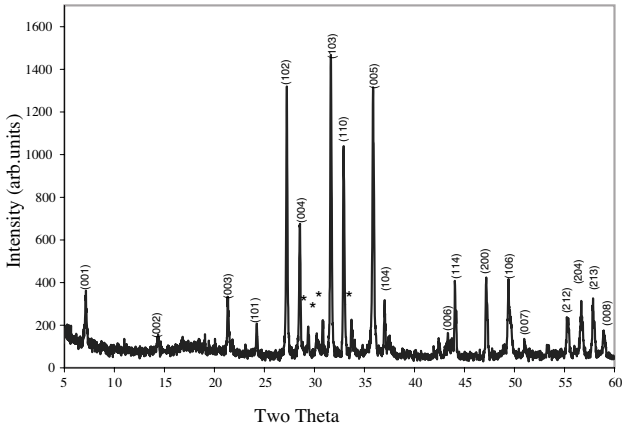


**Figure 1.** X-ray diffraction patterns for the free surface of an as-prepared film sintered at 775° C. The pattern indicates the (Hg,Re)1212 phase is dominant with small amounts of $BaCuO_2$ (marked with "∗").

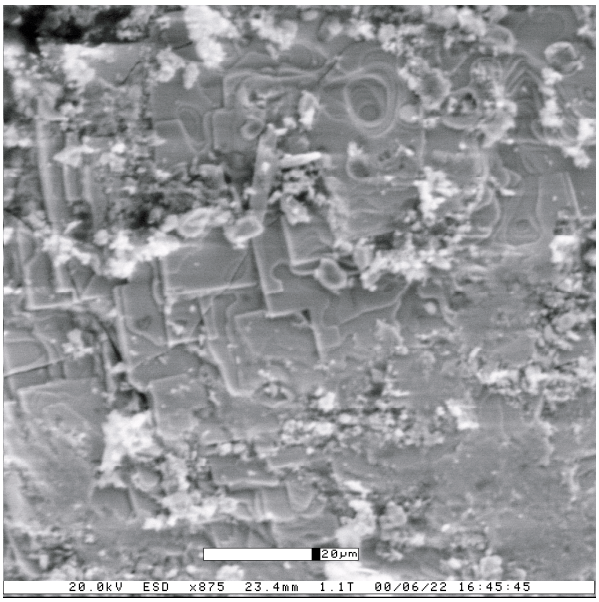


**Figure 2.** Secondary electron micrograph of (Hg,Re)1212 close to the silver interface.

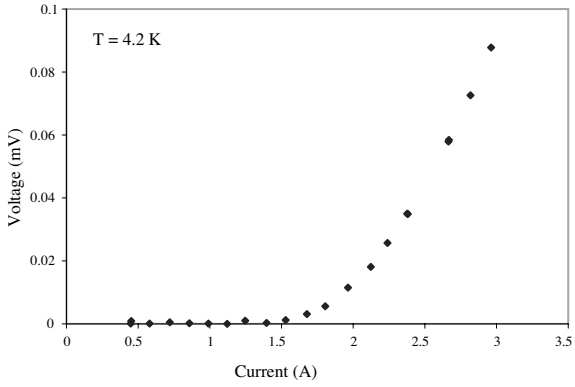


**Figure 3.** Critical current measured at 4.2 K in a self field. The dimensions of the measured film are 1.28 cm × 0.35 cm × 15 µm (average value).

thickness of the film, the average value of $J_c$ is about $3\times10^3$ A/cm$^2$. It should be noted that the maximum local $J_c$, occurring in the smallest thickness (~ 2 µm) region, is at least $2\times10^4$ A/cm$^2$. The transport measurements, although $J_c$ is relatively low, confirmed the presence of superconducting paths. As mentioned above, the randomly oriented grains, growing freely at regions far from the silver surface, and a certain number of voids inhibit transport supercurrent. We hope to increase $J_c$ significantly by further improving the microstructure.

**Acknowledgements:** We would like to thank Ulf Trociewitz and Robert Goddard for their help with the SQUID and ESEM, respectively.

[1] Su, J.H., *et al.,* IEEE Trans. Appl. Supercond., **3,** (2001) (accepted publication).

## The Influence of $BaO_2$ Additions on Microstructure and Superconducting Properties of $Bi_2Sr_2CaCu_2O_{8+\delta}$

Trociewitz, U.P., NHMFL/RWTH Aachen Univ. of Technology
Sahm, P.R., RWTH Aachen Univ. of Technology
Koritala, R.E., Argonne National Laboratory
Bacaltchuk, C., NHMFL/Instituto Militar de Engenharia
Brandao, L., Instituto Militar de Engenharia
Schwartz, J., NHMFL/FAMU-FSU College of Engineering

The effects of Ba additions on $Bi_2Sr_2CaCu_2O_{8+\delta}$ (Bi-2212) superconductors have been investigated focusing on compositional, microstructural, and magnetization properties. $BaO_2$ reacts with the Bi-2212 matrix to form second phase precipitates. SEM micrographs, pole figure analyses, and improved transport properties in self field and high fields up to 17 T suggest significant influence on the development of texture in Bi-2212 due to the addition of $BaO_2$. Magnetization measurements accomplished previously revealed that the pinning properties of optimally $BaO_2$ added Bi-2212 were not affected. To estimate the potential of $BaO_2$

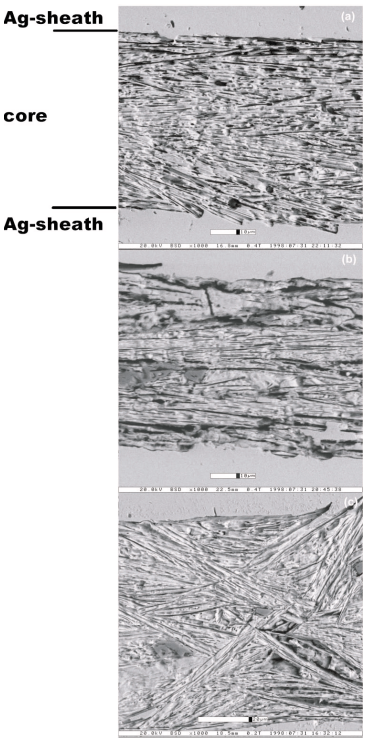


**Figure 1.** In polished and etched cross sections of tape, longer grain growth is clearly visible in the 2.38 wt.% $BaO_2$ added sample (b) compared to the undoped specimen (a). The increased amount of high angle grain boundaries causes inferior transport properties in 3.17 wt.% $BaO_2$ added tape (c).

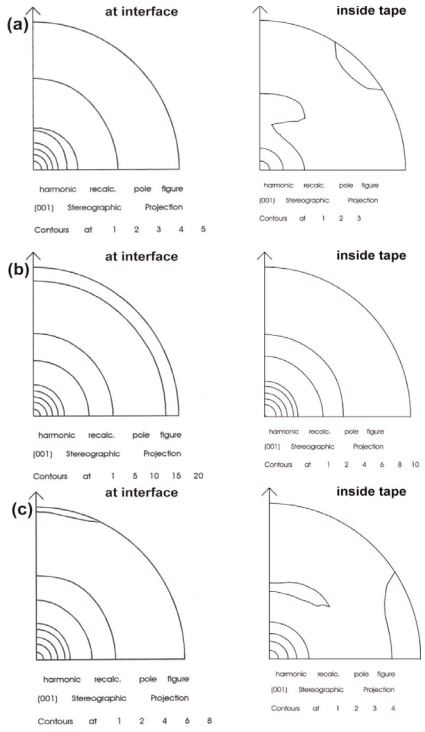


**Figure 2.** Recalculated pole figures of (a) 0.0 wt.%, (b) 2.38 wt.%, and (c) 3.17 wt.% $BaO_2$ added tape samples measured at the interface between Ag and Bi-2212 and close to the midplane of the Bi-2212 core. The data show uniform and pronounced c-axis texture in all samples with the typical degradation towards the center of the core. The 2.38 wt.% added sample, however, shows the highest degree of c-axis texture within the set.

additions to assist the formation of potential pinning sites, TEM investigations were carried out.

In comparison to undoped tape, cross-sections of polished and etched tape samples showed improved microstructure with additions of 2.38 wt.% $BaO_2$ (8 Bi-2212:1 $BaO_2$). With increasing additions above 3.17 wt.% (6:1), the number of high angle grain boundaries increased partially, showing outgrowth of Bi-2212 into the Ag-sheath, (see Fig. 1). This behavior suggested that additional growth mechanisms, probably induced by local concentration gradients of the $BaO_2$, superseded the growth direction enforced by the dimensions of the growth channel in the Ag-sheath. Improved texture properties were also visible in pole-figure analysis on tapes, and the results suggested an optimum of 2.38 wt.% $BaO_2$. With this amount the c-axis texture was the highest at the Ag - Bi-2212 interface as well as around the center plane of the core, (see Fig. 2). EDX spot analysis under the TEM revealed that Ca and Sr were part of the Ba-rich precipitates. Besides $(Ba,Ca,Sr)BiO_3$ smaller phases consisting of (Ba,Sr)O and located closely to the $(Ba,Ca,Sr)BiO_3$ phases were found in some samples. TEM images also revealed that in all investigated samples, the $(Ba,Ca,Sr)BiO_3$ phases were located on the twist boundaries of the Bi-2212 with typical sizes of ≤ 5 μm, (see Fig. 3). Precipitates of these sizes are too large to directly promote pinning in $BaO_2$ added Bi-2212. Irreversibility line measurements, however, showed enhanced pinning of added tape in the temperature regime below 20 K.

**Acknowledgements**: The authors wish to thank Bob Goddard and Ilkay Cubukcu for their valuable help. This project has been supported by funding from the NSF under contract DMR-9527035.

[1] Trociewitz, U.P., *et al.,* Advances in Cryogenic Engineering (Materials), **46B,** 567-574 (2000).

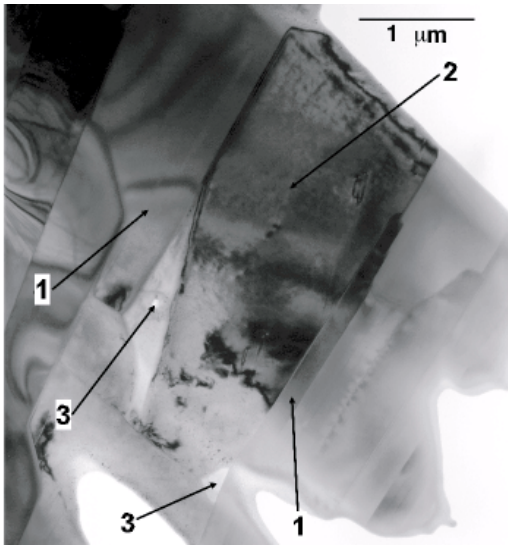


**Figure 3.** TEM image of a 2.38 wt.% $BaO_2$ added tape. The regions marked with the labels were related to following phases, 1: Bi-2212, 2: (Ba,Ca,Sr)$BiO_3$, 3: (Ba,Sr)O.

## Magneto-Optical Imaging Study of Crack Formation in Superconducting Tapes Caused by Applied Strain

van der Laan, D.C., NHMFL/Univ. of Twente, the Netherlands, Faculty of Applied Physics
Davidson, M.W., NHMFL
ten Haken, B., Univ. of Twente, the Netherlands, Faculty of Applied Physics
ten Kate, H.H.J., Univ. of Twente, the Netherlands, Faculty of Applied Physics
Schwartz, J., NHMFL/FAMU-FSU College of Engineering

A Magneto-Optical Imaging (MOI) system[1] is used to study the crack formation in superconducting BSCCO 2223 tapes as a function of applied strain. This will give a better insight into the current limiting mechanisms of these brittle ceramic superconductors.

The installed MOI-system consists of a helium flow cryostat, capable of cooling the sample from room temperature down to 16 K. The sample is placed on a strain bench, which is mounted on a copper cold finger. The strain bench is operated by a stepper motor, installed outside the cryostat. The indicator film with in-plane magnetization[2] is placed on top of the sample. A magnetic field of up to 120 mT is applied by an external magnet. Current leads enable a transport current in the tape. Fig. 1 shows a photograph of the inside of the cryostat.

The silver matrix of the tape is etched away partly to reduce the distance between the filaments and the indicator film. The sample is zero-field-cooled to 30 K, after which an external magnetic field of 120 mT is applied. After the magnetic field is switched off, flux is trapped in the superconductor. Fig. 2 shows the top layer of filaments in an unstrained multi-filamentary tape. The filaments are positioned horizontally in the picture. Three different filaments are visible. Higher intensities of the reflected polarized light in Fig. 2 represent higher densities of trapped flux. The critical current density in the filaments is not homogenous as can be seen from the flux patterns.

Fig. 3 shows the same area of the same sample after a certain amount of strain is applied. The filaments in the picture show transverse cracks. The distance between the cracks is always larger than approximately 200 μm, which is possibly an

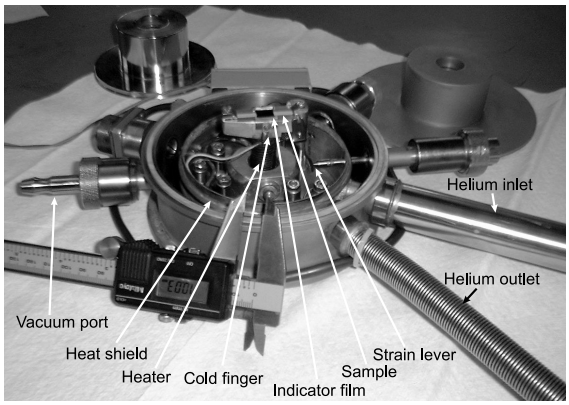


**Figure 1.** The flow cryostat for the MOI-setup.

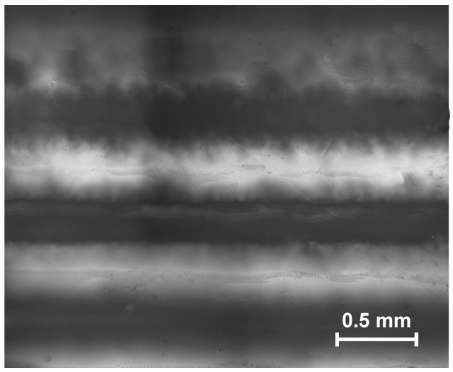


**Figure 2.** MOI image of an unstrained BSCCO 2223 tape.

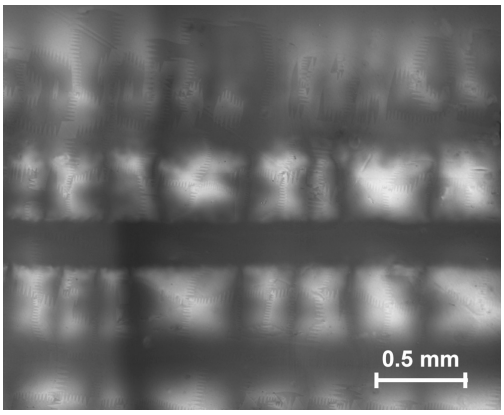


**Figure 3.** MOI image of a strained BSCCO 2223 tape with a well developed crack structure.

indication of the average colony size in the filaments. Before the tape breaks, all filaments have formed cracks which are located approximately 200 μm apart. The development of the crack structure and the average colony size is related to the deformation process of the tape and does not depend on the filament width.

**Acknowledgements.** We would like to thank Korea Institute of Machinery & Materials, Nordic Superconductor Technologies, and Oxford Instruments Inc. Superconducting Technology for making their conductor available to us.

[1] Indenbom, M.V., *et al.,* Physica C, **166**, 486-496 (1990).
[2] Polyanskii, A.A., *et al.,* IEEE Trans. Magn., **26**, 1445-1448 (1990).

## Temperature and Magnetic Field Dependence of the Critical Current of $Bi_2Sr_2Ca_2Cu_3O_x$ Tape Conductors

van der Laan, D.C., NHMFL/University of Twente, the Netherlands, Faculty of Applied Physics
van Eck, H.J.N., University of Twente, the Netherlands, Faculty of Applied Physics
Schwartz, J., NHMFL/FAMU-FSU College of Engineering
ten Haken, B., University of Twente, the Netherlands, Faculty of Applied Physics
ten Kate, H.H.J., University of Twente, the Netherlands, Faculty of Applied Physics

To better understand the mechanisms that limit the critical current in high temperature superconductors, the dependence of the critical current on magnetic field and temperature of a $Bi_2Sr_2Ca_2Cu_3O_x$ tape has been investigated in detail.[1]

The critical current is measured in magnetic fields up to 8 T, at temperatures ranging from 4.2 K to 70 K. The results are compared with existing models that describe the current path as two parallel systems, one depending on weak links and the other on flux pinning. The total critical current is described as:[2]

(1) $$I_C(B,T) = I_{CW}(B,T) + I_{CS}(B,T)$$

The first part of (1) describes the critical current of the weak link path. A relation based on intergrain pinning[3] is used for this current path, as given by equation (2). Equation (3) describes the strong link current path, which depends on intragrain pinning.[4]

(2) $$I_{CW}(B,T) = \frac{I_{CW}(0,T)}{1+\left(\frac{|B|}{B_0(T)}\right)^{\beta}}$$

(3) $$I_{CS}(B,T) = I_{CS}(0,T)\exp\left(-\left(\frac{B}{B_{SC}(T)}\right)^{\alpha(T)}\right)$$

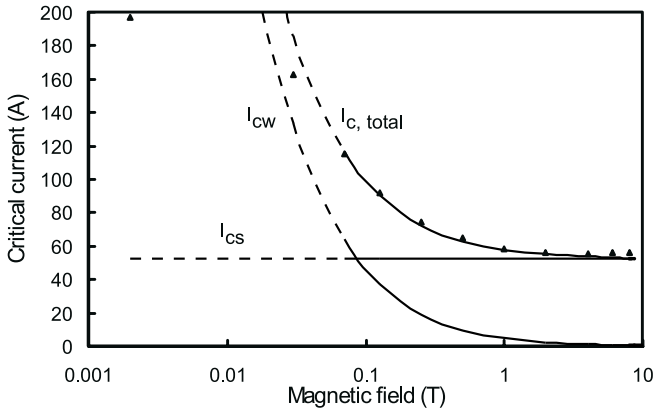


**Figure 1.** Critical current as function of magnetic field and temperature.

Fig. 1 shows the measured critical current as function of applied magnetic field at 4.2 K. The weak-link critical current and the strong-link critical current given by equations (1) and (2) are included in the figure.

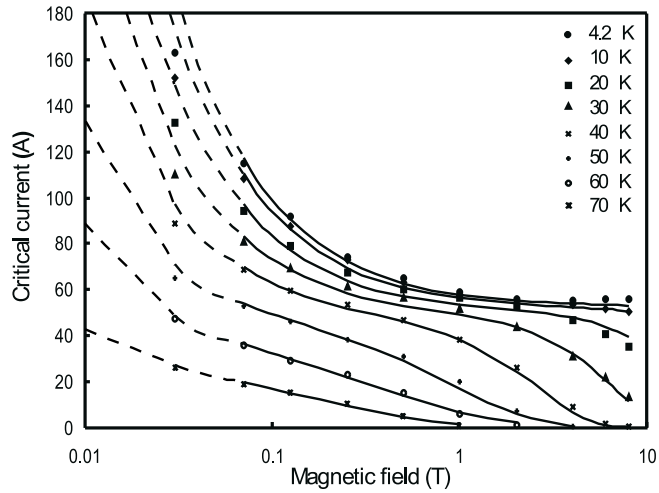


**Figure 2.** Critical current as function of magnetic field and temperature.

Fig. 2 shows the critical current of the tape, measured as function of applied magnetic field for different temperatures. The critical current at low magnetic fields is reduced drastically by the self-field of the superconductor. At intermediate magnetic fields, the field dependence of the critical current is dominated by weak links, while at higher fields it is dominated by the strongly linked current path, and depends on flux pinning. The model described by (1) is included in the figure as indicated by the solid lines.

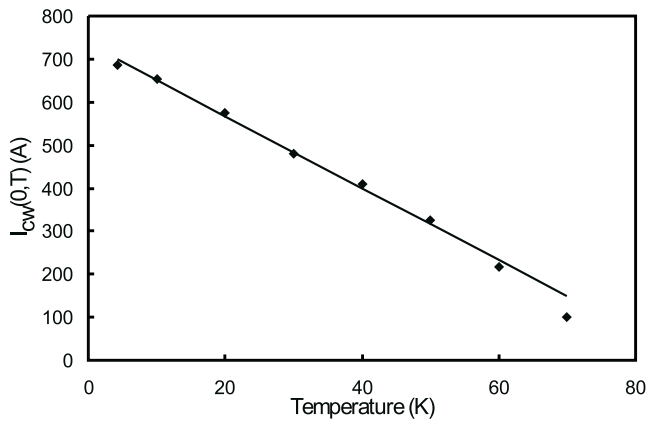


**Figure 3.** Temperature dependence of the weak-links critical current at zero magnetic field.

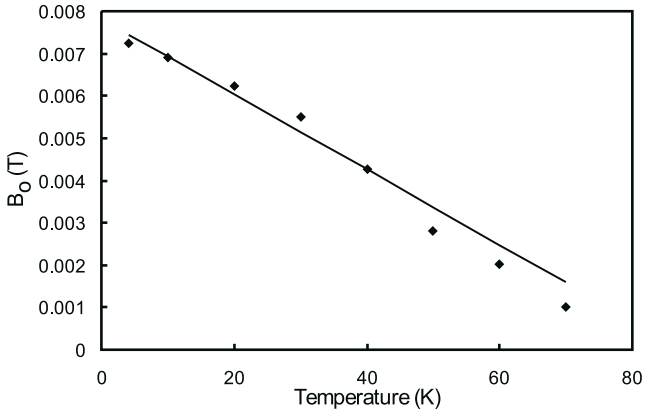


**Figure 4.** Temperature dependence of $B_0$.

To clarify the models used to describe the measurements, the temperature dependence of the parameters used in the models is studied. Fig. 3 and 4 show the temperature dependence of $I_{CW}$ at zero magnetic field and the characteristic field $B_0$ of the weak links. These parameters show a linear temperature dependence and both vanish at a temperature of approximately 87 K, where the critical current of the weak link path is reduced to zero. The termination of the weak link current path at 87 K indicates that the weak links may be formed by remnant $Bi_2Sr_2CaCu_2O_x$ phase at the grain boundaries.


[1] van der Laan, D.C., *et al.,* to be published in the IEEE Transactions on Applied Superconductivity.
[2] Huang, Y.K., *et al.,* Physica C, **309**, 197-202 (1998).
[3] Müller, K.-H., *et al.,* Physica C, **158**, 69-75 (1989).
[4] Feigel'man, V.M., *et al.,* Physical Review B, **41**, 13, 8986-8990 (1990).

## Compression-Tension Stress-Strain-Ic Measurements of Bi-2223 Tapes

Viouchkov, Y., NHMFL
Schwartz, J., NHMFL/FAMU-FSU College of Engineering

Understanding the mechanical properties of HTS tapes is an important aspect for the design and development of magnet applications. Coils are subject to complex strain states due to fabrication, thermal mismatch, and operation. Here we report on a novel method developed at the NHMFL for measuring the compressive stress-strain-Ic behavior at 77 K and room temperature.

When performing axial compression experiments on HTS tapes, buckling is a concern. A second order homogeneous differential equation of the static equilibrium force P and the bending moment M depict the critical load and deflection u of a buckled sample:

$$-M=-P\upsilon;\ EI\upsilon''+P\upsilon=0 \qquad (1)$$

The general solution of equation (1) for a sample with fixed ends in calipers gives the smallest critical load:

$$P_{cr}=n^2 4\pi^2 EI/L^2 \qquad (2)$$

To increase the critical load, it is necessary to either reduce the length L of the sample, which is limited by the resolution of the testing equipment, or increase n by controlling the sample deflection.

To control the deflection of the tape during compression, a support rig was developed. The rig is assembled from two symmetrical triangular-shape blocks with channels for the sample (Fig. 1). A linear tester originally developed for tensile testing was used to measure the compressive stress-strain curves. Measurements were carried out for four scenarios: compression and tension at 77 K and room temperatures. HTS samples were supplied by American Superconductor Corporation. Two types of Ag-alloy sheathed conductors were studied: bare tape and conductor reinforced by laminated stainless steel.

To measure Ic as a function of stress, discrete loads were applied to each sample. Ic was measured at 77 K after deformation along with a reference sample that determined Ico, the critical current at zero load.

Fig. 2 shows tension-compression stress-strain-Ic data of laminated Bi-2223 superconductor deformed at 77 K and room temperature. No degradation on Ic was found on bare tapes under any testing condition without destroying the mechanical integrity of the outer sheath.

**Acknowledgements:** This work was supported by the Office of Naval Research.

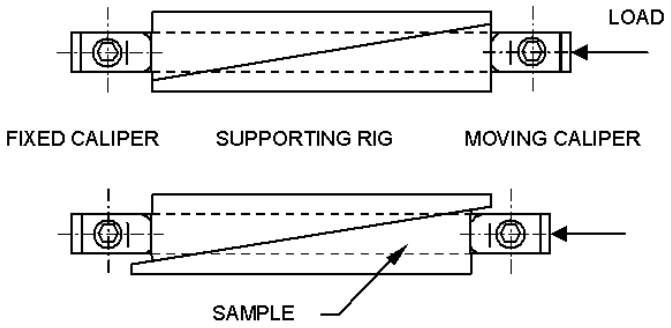


**Figure 1.** Schematic view of the support rig for compressive tests.

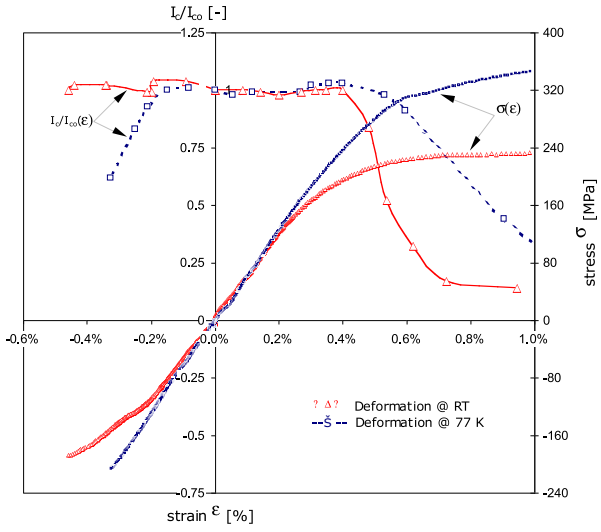


**Figure 2.** Tension-compression stress-strain-Ic data of laminated Bi-2223 superconductor.

## High Field Test Coil for Navy 25 MW Motor Program

Voccio, J.P., American Superconductor Corporation
Schwartz, J., NHMFL
Weijers, H., NHMFL

The objective of this test was to determine if the coils for the 25 MW Navy motor program can withstand the high radial, Lorentz stresses developed in the motor. Based on the preliminary design and analysis of these motor coils, the peak radial stress is ~200 psi. Data previously taken on unlaminated conductor indicated that damage could occur as low as 500 psi; however, this motor would be fabricated using laminated conductor.

Two test coils were fabricated for testing in the 20 T, 20 cm bore resistive magnet at NHMFL. Each coil was initially tested and cycled at American Superconductor Corporation (AMSC), then sent to NHMFL for high field testing. The testing indicated that damage occurred at a much higher (9 x) stress level than the design stress. In addition, the mechanism of failure was most probably not due to high radial stress at the ID of the coil, but rather local damage of the OD turn. Therefore, the demonstrated radial stress of 1800 psi serves as a lower limit for the strength of this coil.

**Acknowledgements:** The authors wish to thank Scott Young, Frances Stephens, and Dave Johnson of AMSC for their work in fabricating the test coil and Bob Givin for his help in initial 4 K cycling. This work was sponsored by the Office of Naval Research under a development contract.

## Characterization of $Nb_3Sn$ Superconductors

Walsh, R.P., NHMFL
Faik, H., INSA
Haslow, M., NHMFL
Toplosky, V.J., NHMFL

Experiments have been conducted to develop an improved test method for measuring a superconductor's critical current in a magnetic field as a function of axial strain. Of the technical superconductors, members of the A15 family have high critical temperatures and some of the highest critical fields (pure-strain free $Nb_3Sn$ $T_c$=18.5 K and $B_{c2}$ (0)=28 T). In practice, these parameters are lower because the compound is under mechanical stress caused by strain during low temperature, high magnetic field service. The thermal contraction of the composite wire creates a residual compressive strain on the $Nb_3Sn$ (of about 0.31 %), thus critical current density is degraded at zero applied strain.

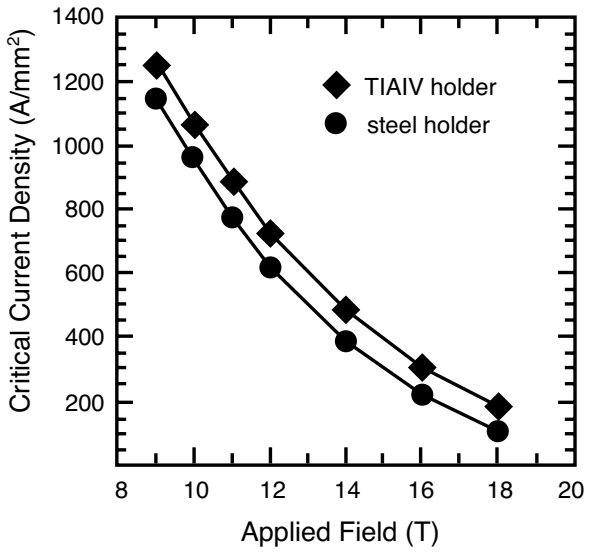


**Figure 1.** Critical current density of $Nb_3Sn$ wire soldered to different substrates (Ref. 1).

The application of a tensile strain counteracts the compressive strain resulting in an increase of $J_c$, but after a certain limit, it degrades the superconducting properties until the filament failure causes permanent degradation. The strain sensitivity of the performance of the

superconductor necessitates careful, accurate measurement of current transport properties. Measurements are complicated by the need to support wire samples to react transverse stress without influencing axial strain. Wires can be soldered to substrates that will influence the thermal strain from cool-down. Here we studied the effect of various substrate materials that have a range of thermal contractions. The critical current density as a function of applied field is shown in Fig. 1. Fig. 2 shows the stress vs. strain characteristics of the composite wire ($Nb_3Sn$ Hybrid A Coil wire) measured at 4 K. The large bore, high field, resistive magnet (195 mm dia, 20 T) here at NHMFL provides opportunity to test $J_c$ vs. strain on single wires with their axis transverse to the applied field. Currently an axial strain rig is being developed to enable $J_c$ vs. strain tests of wires in a high magnetic field.

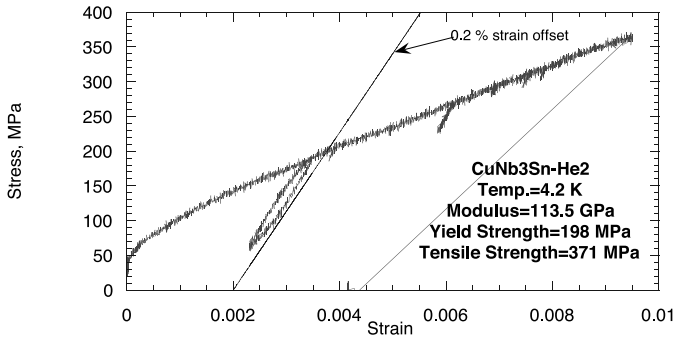


**Figure 2.** Typical stress vs. strain curve of $Nb_3Sn$/Cu wire at 4 K.

[1] Hentges, R., *et al.,* IEEE Trans. on Applied Superconductivity, **9** (2), 1444-1446, June (1999).